Bridging the Gap in Ophthalmic AI: MM-Retinal-Reason Dataset and OphthaReason Model toward Dynamic Multimodal Reasoning

Ruiqi Wu, Yu'ang Yao, Tengfei Ma, Chenran Zhang, Na Su, Tao Zhou, *Senior Member, IEEE*, Geng Chen, *Senior Member, IEEE*, Wen Fan*, Yi Zhou*, *Senior Member, IEEE*

***Abstract*—Multimodal large language models (MLLMs) have recently demonstrated remarkable reasoning abilities with reinforcement learning paradigm. Although several multimodal reasoning models have been explored in the medical domain, most of them focus exclusively on basic reasoning, which refers to shallow inference based on visual feature matching. However, real-world clinical diagnosis extends beyond basic reasoning, demanding reasoning processes that integrate heterogeneous clinical information (such as chief complaints and medical history) with multimodal medical imaging data. To bridge this gap, we introduce MM-Retinal-Reason, the first ophthalmic multimodal dataset with the full spectrum of perception and reasoning. It encompasses both basic reasoning tasks and complex reasoning tasks, aiming to enhance visual-centric fundamental reasoning capabilities and emulate realistic clinical thinking patterns. Building upon MM-Retinal-Reason, we propose OphthaReason, the first ophthalmology-specific multimodal reasoning model with step-by-step reasoning traces. To enable flexible adaptation to both basic and complex reasoning tasks, we specifically design a novel method called Uncertainty-Aware Dynamic Thinking (UADT), which estimates sample-level uncertainty via entropy and dynamically modulates the model's exploration depth using a shaped advantage mechanism. Comprehensive experiments demonstrate that our model achieves state-of-the-art performance on both basic and complex reasoning tasks, outperforming general-purpose MLLMs, medical MLLMs, RL-based medical MLLMs, and ophthalmic MLLMs by at least 24.92%, 15.00%, 21.20%, and 17.66%. Project Page: link.**

***Index Terms*—Multimodal Reasoning, Reinforcement Learning, Ophthalmology, Dynamic Reasoning**

I. Introduction

MEDICAL diagnosis is a complex process that fundamentally relies on logical inference and clinical expertise. In ophthalmology, this challenge is more pronounced, demanding the integration of diverse imaging modalities and extensive clinical contexts. Recent advancements in multimodal large language models (MLLMs) [19] [13] [11] [44] [31] offer a powerful solution. By incorporating explicit reasoning traces, reinforcement learning (RL)-based models can significantly improve interpretability and reliability thus fostering safer and more trustworthy medical artificial intelligence (AI).

Most existing multimodal medical reasoning models [37] [23] [12] [55] are tailored for general medicine, pathology and radiology. However, due to the lack of large-scale and well-annotated ophthalmology-specific visual question answering (VQA) data, the development of ophthalmic reasoning models falls behind. Moreover, existing models primarily focus on basic tasks with simple queries as illustrated in Fig. 1(a)(b). The former often involves questions of limited clinical relevance, such as imaging modality recognition and orientation identification, while the latter relies on visual feature matching with shallow reasoning. Though effective for basic diagnoses, such models often fail to address the complex reasoning required in real clinical practice. Unlike standardized benchmarks, real-world clinical scenarios involve ambiguous symptoms and comorbidities that require more than knowledge matching on a single imaging modality [45]. Accurate diagnosis often requires diverse imaging modalities and heterogeneous clinical information, such as chief complaint (CC), history of present illness (HPI), symptom progression, and physical examination (PE) [38] (see Fig. 1 (c)), which is not only helpful in diagnosing common diseases but essential when confronting complex or rare conditions.

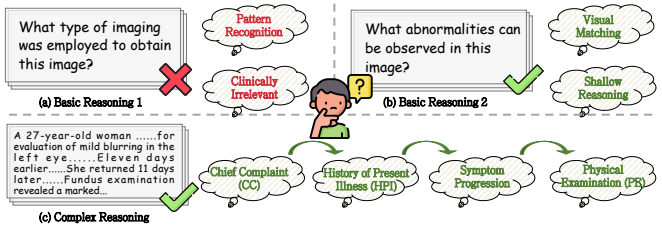

Fig. 1: Comparison between basic and complex reasoning tasks. (a) Some basic tasks focus on modality or organ recognition, which are clinically irrelevant. (b) Other basic tasks pertain to diagnosis, involving shallow reasoning due to limited information in the question. (c) Complex tasks incorporate heterogeneous real-world clinical information, enabling deeper reasoning. Our dataset includes both (b) and (c) tasks, and OphthaReason dynamically adapts to varying reasoning complexities.

These limitations underscore the necessity of developing multimodal medical reasoning models that can handle multi-source, heterogeneous reasoning tasks with varying levels of diagnostic complexity. However, most existing approaches treat all reasoning tasks indiscriminately [39] [12] [23] [55], without adapting the model's exploratory capabilities to varying task complexity. This limits their ability to cope with heterogeneous diagnostic scenarios, resulting in low reasoning efficiency and inadequate exploration depth. Although QoQ-Med [10] attempts to address the challenge of heterogeneous data by framing it as a domain imbalance problem, its effectiveness is constrained by reliance on pre-defined domains and a coarse-grained, cluster-level estimation strategy,

R. Wu, Y. Yao, T. Ma, C. Zhang, and Y. Zhou are with the School of Computer Science and Engineering, Southeast University, Nanjing, China.

N. Su, and W. Fan are with the Department of Ophthalmology, The First Affiliated Hospital of Nanjing Medical University, Nanjing, China.

T. Zhou is with the School of Computer Science and Engineering, Nanjing University of Science and Technology, Nanjing, China.

G. Chen is with the School of Computer Science, Northwestern Polytechnical University, Xi'an, China.

*Corresponding authors: *Yi Zhou* (yizhou.szcn@gmail.com) and *Wen Fan*.

underscoring the need for reasoning models with fine-grained, sample-level dynamic thinking capabilities.

To address these challenges, we introduce MM-Retinal-Reason, the first ophthalmology-specific multimodal reasoning dataset designed for expert-level diagnostic tasks, integrating both basic and complex reasoning tasks to reflect real-world clinical scenarios. MM-Retinal-Reason is built from real-world data collected from 45 public datasets and PubMed Central (PMC), supplemented with reasoning trajectories. It comprises 4 types of questions, including true/false questions, single-answer multiple-choice, multiple-answer multiple-choice, and open-ended questions, covering over 100 common and rare ophthalmic abnormalities. MM-Retinal-Reason consists of four components: basic reasoning VQA, chain-of-thought (CoT) reasoning trajectories, image-caption pairs, and complex reasoning VQA, providing comprehensive supervision for the training and evaluation of ophthalmic MLLMs across the full spectrum of perception and reasoning.

Furthermore, we propose OphthaReason, a multimodal medical reasoning model for ophthalmic diagnosis that supports dynamic reasoning across tasks ranging from basic questions to complex scenarios. It adopts a three-stage training pipeline consisting of vision-language alignment, CoT supervised fine-tuning (SFT), and reinforcement learning, which together enable perception enhancement, stepwise reasoning, and clinical decision-making. Specifically, we develop Uncertainty-Aware Dynamic Thinking (UADT), which leverages sample-wise entropy to guide adaptive reasoning. Based on each sample's uncertainty, UADT encourages broader exploration of uncertain challenging cases while mitigating excessive updates on confident trivial ones. This mechanism allows OphthaReason to simulate the flexible cognitive process of human experts, dynamically adjusting exploration depth to match the complexity of each sample.

In summary, our key contributions are: (1) The construction of MM-Retinal-Reason, which is the first multimodal ophthalmic dataset designed for both basic and complex reasoning tasks, providing comprehensive supervision across perceptual understanding and reasoning processes. (2) The introduction of OphthaReason, which is the first RL-based multimodal ophthalmic reasoning model to the best of our knowledge. It is trained through a three-stage pipeline to enhance both perceptual understanding and reasoning capability. (3) The creation of Uncertainty-Aware Dynamic Thinking, which dynamically promotes deeper exploration for uncertain samples while applying minimal updates to certain ones based on sample-level entropy. (4) Extensive experiments demonstrate that OphthaReason consistently enhances performance across diverse imaging modalities and varying reasoning complexity, achieving 24.92%, 15.00%, 21.20%, and 17.66% improvements over general-purpose, medical, RL-based medical, and ophthalmic MLLMs of 3-4 times its size.

II. Related Work

A. Multimodal Medical Benchmarks

High-quality multimodal medical benchmarks are essential for developing medical reasoning models. Several datasets have been introduced to support vision-language learning in the medical domain, such as VQA-Med [4], PMC-VQA [56], and OmniMedVQA [16]. These benchmarks primarily focus on basic, single-image VQA tasks like disease or modality identification, failing to capture the contextual complexity of real-world clinical diagnosis. With the advancement of MLLMs, several benchmarks have begun to incorporate more complex reasoning. MedXpertQA-MM [58] introduces expert-level medical reasoning questions, yet lacks explicit reasoning chains that make the decision-making process interpretable. MedFrameQA [54] integrates multi-image inputs and reasoning processes. However, it falls short in modeling a complete clinical encounter, lacking crucial patient information such as clinical history and physical examination findings. To fill this gap, we propose MM-Retinal-Reason, spanning from basic to complex reasoning tasks with explicit reasoning trajectories.

B. Multimodal Medical Reasoning Models with RL

Reinforcement learning (RL) has played a pivotal role in advancing multimodal medical reasoning. These models can be broadly categorized into two streams: generalist models like MedVLM-R1 [37], Med-R1 [23], QoQ-Med [10], lingshu-RL [52], MedCCO [39], which target broad medical reasoning tasks, and specialist models tailored to specific clinical domains such as ChestX-Reasoner [12], BoxMed-RL [20] for radiology and Patho-R1 [55], PathVLM-R1 [48] for Pathology. Nonetheless, these advancements have not yet been extended to ophthalmology. To bridge this gap, we introduce OphthaReason, the first RL-based ophthalmic reasoning model to the best of our knowledge. Unlike prior approaches that apply uniform exploration strategies across all samples, OphthaReason dynamically modulates exploration depth based on sample uncertainty, improving both robustness and accuracy.

C. Ophthalmic VLMs and MLLMs

While early ophthalmic Vision-Language Models (VLMs) like FLAIR [42], KeepFIT [51] [50], RetiZero [46], and EyeCLIP [41] excelled at image understanding, they lacked generative and instruction-following capabilities. This led to the development of ophthalmic Multimodal Large Language Models (MLLMs) to bridge this gap [32]. RetinalGPT [57] integrates retinal images with structured vascular fractal features through feature alignment and mixup instruction tuning. EyeCareGPT [27] utilized adaptive resolution and dense connector for fine-grained analysis. FundusExpert [30] enabled positioning-diagnosis collaboration, directly linking image regions to text. However, most ophthalmic MLLMs target single imaging modality analysis and are designed for basic VQA tasks, making them fail to handle the complex reasoning required in real-world clinical scenarios. Moreover, they generally lack an adaptive reasoning mechanism to regulate the exploration progress based on sample uncertainty.

III. MM-Retinal-Reason

MM-Retinal-Reason is an ophthalmic multimodal dataset that provides comprehensive data across a full spectrum of

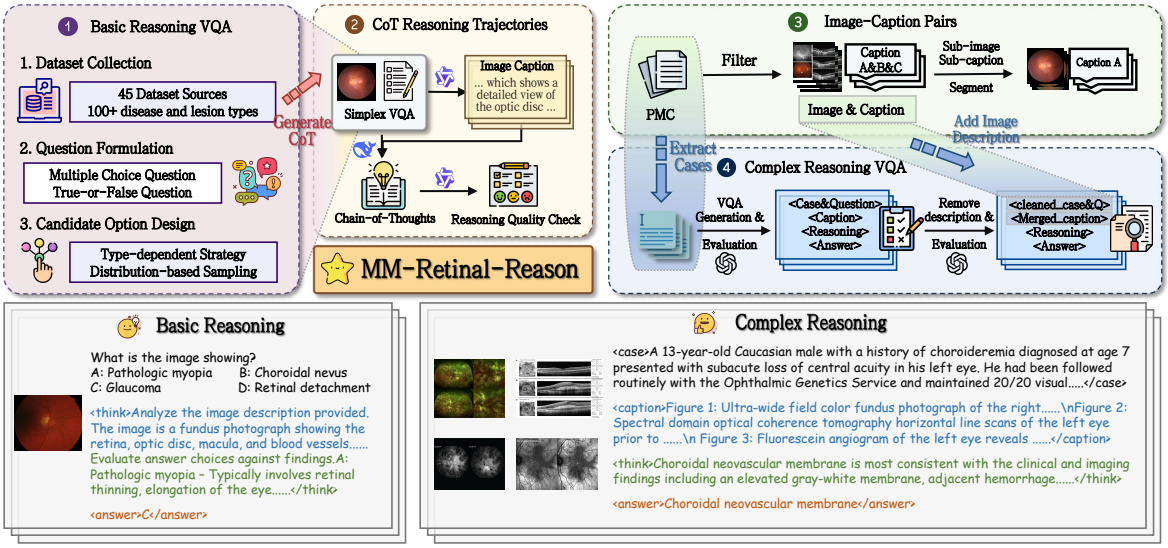

Fig. 2: Construction pipeline of MM-Retinal-Reason and examples from the VQA subset. MM-Retinal-Reason consists of four interconnected components covering a wide range of perception and reasoning tasks. The VQA subset includes basic tasks for fundamental visual reasoning and complex tasks simulating real-world diagnostics with heterogeneous clinical information. This design enables OphthaReason to master tasks of varying cognitive complexity.

perception and reasoning tasks, featuring explicit reasoning traces aligned with real-world clinical scenarios. The dataset comprises four components: basic reasoning VQA, CoT reasoning trajectories, image-caption pairs, and complex reasoning VQA. The overall curation workflow is shown in Fig. 2.

A. Part 1: Basic Reasoning VQA

Due to the lack of large-scale ophthalmic VQA datasets with multiple imaging modalities, we create this subset from 45 public fundus classification datasets, including 55,224 VQA pairs for Color Fundus Photography (CFP), 34,159 for Fundus Fluorescein Angiography (FFA), and 131,985 for Optical Coherence Tomography (OCT), covering over 100 disease and lesion types.

For question formulation, we adopt templates from PubMedVision [6], MeCoVQA-Complex [18], and DeepSeek-R1 [13], including single-answer, multi-answer multiple-choice questions (MCQs), and binary true/false questions.

Regarding candidate option design, we employ strategies dependent on dataset type. For single-label datasets with common diseases (e.g., LAG [26], RetinalOCT-C8 [34]), we unify categories across datasets to form a shared candidate option pool, increasing question difficulty by expanding the choice space. For multi-label datasets with numerous diverse and rare conditions (e.g., RFMiD [36], STARE [14] [15]), we retain original labels to preserve inherent complexity.

To ensure an appropriate candidate option sampling probability, our label pool design is guided by the label distribution of original dataset. This prevents models from exploiting shortcuts by eliminating rare or unlikely answers and selecting the most frequently correct choice.

B. Part 2: CoT Reasoning Trajectories

To better stimulate the model's reasoning capabilities, we construct CoT reasoning trajectories for the basic reasoning VQA subset in Section III-A. The final subset includes 10,270 CFP, 3,274 FFA, and 2,343 OCT CoT reasoning trajectories.

Following Vision-R1 [17], we first use Qwen2.5-VL-72B [3] to convert visual content into textual descriptions, then prompt DeepSeek-R1 to generate CoT data incorporating both visual cues and step-by-step reasoning. We then conduct a quality check on the generated CoT, retaining only samples with correct answers. Additionally, to enhance the quality of the reasoning process, we employ an MLLM-based validation to assess the generated content across five dimensions: image description clarity, reasoning transparency, reasoning validity, reasoning integrity, and diagnostic rigor.

C. Part 3: Image-Caption Pairs

The image-caption subset comprises 80,520 pairs, spanning diverse ophthalmic imaging modalities, including CFP, OCT, FFA, Computed Tomography (CT), Slit-Lamp, Ultrasound, and others. To construct this subset, we collect ophthalmology-related articles and associated images from PMC up to June 20, 2025, which are subsequently filtered by modality names. Compound figures are split either by morphological operations or by Dab-DETR [29]. Subcaptions are parsed with Qwen2.5-VL-72B and aligned to subfigures using spatial rules.

D. Part 4: Complex Reasoning VQA

Most medical VQA datasets are limited to single-image input and basic reasoning (see Fig 1). While some explore multi-image input or complex reasoning, they rarely integrate all key elements: multimodal multi-image input, clinically relevant questions with heterogeneous patient information, and explicit reasoning trajectories. To bridge this gap, we construct a complex reasoning VQA subset based on real ophthalmology case reports from PMC, resulting in a total of 5,027 complex reasoning VQA samples. Among them, 400 are reserved as a test set that covers a comprehensive range of diseases.

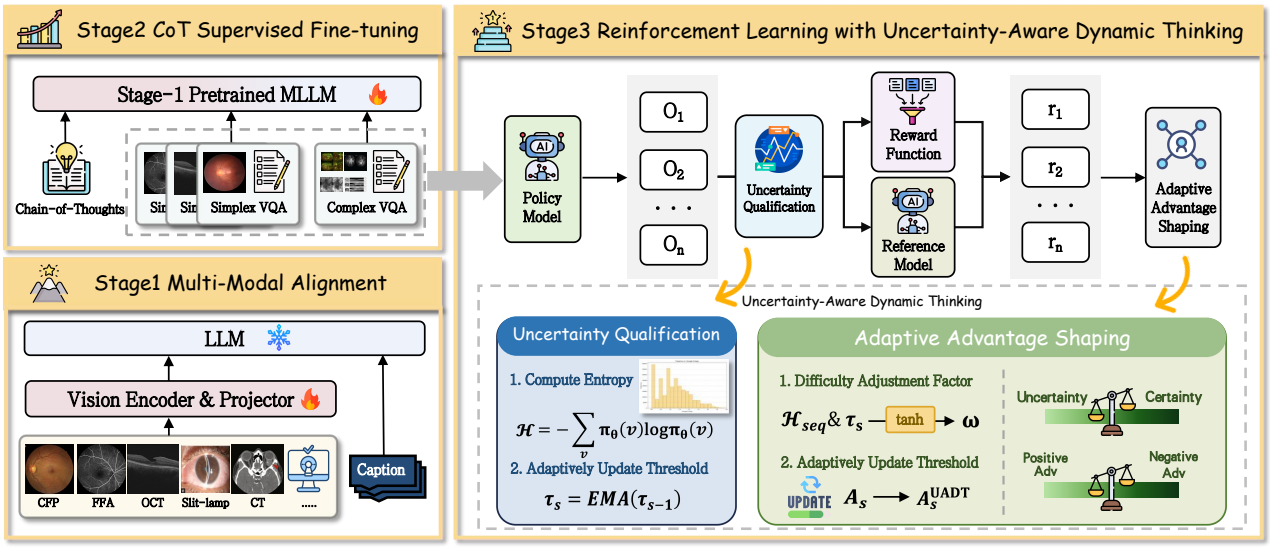

Fig. 3: Overview of OphthaReason. OphthaReason adopts a three-stage training framework consisting of multimodal alignment, CoT supervised fine-tuning, and reinforcement learning. In the third stage, the Uncertainty-Aware Dynamic Thinking mechanism is introduced for adaptive exploration across samples with varying uncertainty levels. OphthaReason demonstrates strong capability in both basic image-based diagnostic reasoning and complex clinical contextualized reasoning, aligning with the reasoning patterns of ophthalmologists.

- **Step 1: Raw Complex VQA Generation.** We first apply rule-based filtering to select cases. Inspired by [49], we develop a tailored pipeline to create structured VQA by o4-mini [35]. Each entry contains `<Presentation & Question>`, `<Reasoning Trace>`, `<Image Caption>`, and `<Answer>`. To ensure information completeness for subsequent evaluation, image descriptions are temporarily retained in `<Presentation & Question>`, which will be removed in Step 3.
- **Step 2: Component-wise Quality Evaluation.** We conduct an automated evaluation using o4-mini to assess the generated VQA across eight metrics under three principal themes: case completeness, reasoning depth, and clinical significance, following the rubric in [49].
- **Step 3: Visual Information Extraction.** After selecting valid samples from Step 2, we prompt o4-mini to remove redundant text in `<Presentation & Question>`that overlaps with `<Image Caption>`. Then, we use Qwen-Plus to align each case with its corresponding figures and employ o4-mini to enrich the `<Image Caption>`with data from Section III-C.
- **Step 4: Hallucination Evaluation.** We assess the source fidelity to the original case report by extending the approach in [49]. Samples with low scores are excluded.

The primary distinction between our dataset and MedCaseReasoning [49] is that MedCaseReasoning contains only textual QA, whereas we provide a multimodal, multi-image ophthalmic VQA dataset. This dataset promotes a deeper level of multimodal understanding and reasoning, aligning more closely with real-world medical scenarios.

IV. OphthaReason

Building upon the MM-Retinal-Reason, we further introduce OphthaReason, a three-stage multimodal reasoning model designed for the full spectrum of ophthalmic diagnosis, from basic image-based reasoning to complex, clinically-simulated reasoning. A key component of OphthaReason is Uncertainty-Aware Dynamic Thinking (UADT), a novel mechanism that enables the model to dynamically adapt its exploration depth to tasks of varying difficulty. We developed two versions of OphthaReason for the community, building upon Qwen2.5-VL-3B-Instruct and InternVL3-2B, which are two of the most prominent general-purpose MLLMs with leading reasoning capability. The framework of OphthaReason is illustrated in Fig. 3.

A. Stage 1: Foundational Vision-Language Alignment

While general-purpose MLLMs demonstrate strong foundational vision-language alignment, their capability for interpreting specialized ophthalmic images remains underdeveloped. Furthermore, the text-centric architecture limits their visual perception [47], weakening the contribution of visual features in reasoning space. To address these issues, we first enhance ophthalmic vision-language alignment using the image-caption pair subset from the MM-Retinal-Reason and MM-Retinal datasets [51] [50]. We selectively fine-tune only the vision encoder and projector, leaving the LLM frozen to prevent its advanced language modeling from being degraded by the simple caption data.

B. Stage 2: Activating Reasoning via CoT-SFT

Prior works [17] [44] [43] have demonstrated that supervised fine-tuning on CoT data effectively unlocks the reasoning abilities of MLLMs through step-by-step logical processes. In the second stage, we fine-tune the whole model using a combination of the reasoning trajectories from both basic and complex reasoning VQA subsets. This preserves the model's structured thinking ability, which would be undermined if solely fine-tuned on final answers. Given a sample consisting

of a set of K images $X = \{x_1, x_2 \ldots, x_K\}$ (where $K \geq 1$), a question q, a CoT reasoning trajectory r, and a final answer a, the training objective is to maximize the likelihood of generating the correct reasoning trace and answer:

$$\mathcal{J}_{\text{SFT}}(\theta) = -\mathbb{E}[(X, q, r, a) \sim \mathcal{P}] \sum_{t=1}^{T} \log \pi_\theta(y_t | X, q, y_{<t}), \quad (1)$$

where $\mathcal{P}$ represents the dataset, the image number $K = 1$ for basic reasoning tasks, and $K \geq 1$ for complex reasoning tasks. The term y is the concatenated sequence of reasoning trace r and answer a, t indexes the token position in the sequence, and T denotes the total sequence length.

C. Stage 3: Reasoning Enhancement with Uncertainty-Aware Dynamic Thinking RL

1) Policy Optimization: Building on the reasoning-activated model in stage 2, we apply Group Relative Policy Optimization (GRPO) [40] to further enhance the model's reasoning ability. Given an input sample $(\{x_1, x_2, \ldots, x_K\}, q, r, a)$ (where $K \geq 1$), the policy model π_θ generates G candidate outputs $O = \{o_1, o_2, \ldots, o_G\}$. Each candidate output o_i is then evaluated by the reward function to yield a corresponding reward r_i, forming the reward set $R = \{r_1, r_2, \ldots, r_G\}$. Instead of an additional value model, GRPO computes the advantage directly by the following formulation:

$$A_i = \frac{r_i - \text{mean}(\{r_1, r_2, \ldots, r_G\})}{\text{std}(\{r_1, r_2, \ldots, r_G\})}. \quad (2)$$

Then GRPO optimizes the policy model by maximizing the following objective:

$$\begin{aligned} \mathcal{J}_{\text{GRPO}}(\theta) = \mathbb{E}[(X, q, a) \sim \mathcal{P}, \{o_i\}_{i=1}^{G} \sim \pi_{\theta_{old}}(O|X, q)] \\ \frac{1}{G} \sum_{i=1}^{G} \Big\{ \min \Big[\frac{\pi_\theta(o_i|X,q)}{\pi_{\theta_{old}}(o_i|X,q)} A_i^{\text{UADT}}, \\ \text{clip}\Big(\frac{\pi_\theta(o_i|X,q)}{\pi_{\theta_{old}}(o_i|X,q)}, 1-\varepsilon, 1+\varepsilon \Big) A_i^{\text{UADT}} \Big] \\ - \beta D_{KL}[\pi_\theta || \pi_{\text{ref}}] \Big\}, \end{aligned} \quad (3)$$

where A_i^{UADT} is the advantage shaped by Uncertainty-Aware Dynamic Thinking (UADT) described in Sec. IV-D, which adaptively adjusts the magnitude of the original advantage A_i from Eq. 2. The hyperparameters ε and β set the clipping range and regulate the strength of the KL divergence penalty, respectively. The KL divergence serves as a regularization term that constrains the policy model π_θ, preventing excessive deviation from the original policy π_{ref}.

2) Reward Function: We employ a composite reward function for each task, comprising a format reward and an accuracy reward, with specific criteria tailored to the task type.

- **Format Reward.** This is a binary score for structural adherence. For all tasks, it verifies whether reasoning is encapsulated in <think ></think >tags, followed by the answer in <answer></answer >tags. For open-ended questions, it additionally requires the model to first generate an image description within <caption ></caption >tags to encourage stronger attention on visual content in complex reasoning tasks.
- **Accuracy Reward.** This score measures content correctness. For MCQ task, we compute an IoU score $R_{IoU} = (y \cap \hat{y})/(y \cup \hat{y})$ between the predicted answer $\hat{y}$ and the ground-truth answer y, which offers a robust measure for partially correct responses that a simple exact-match would fail. For open-ended questions, the reward is calculated as the weighted score of the model's Top-5 answers, which are averaged across BLEU, ROUGE, and METEOR to simultaneously evaluate precision, recall, and synonym-aware alignment.

D. Uncertainty-Aware Dynamic Thinking

Vanilla GRPO treats all samples uniformly regardless of task difficulty, thus lacking a dynamic mechanism to adapt its exploratory behavior to varying levels of diagnosis case complexity. When confronted with a mixture of basic and complex reasoning problems, this one-fits-all strategy can be suboptimal, leading to insufficient exploration for complex problems and excessive optimization for simpler ones.

Thus, we propose Uncertainty-Aware Dynamic Thinking (UADT), a novel advantage-shaping mechanism from an entropy perspective, leveraging sample-level uncertainty to regulate the learning process dynamically. For challenging, high-uncertainty tasks, it introduces an entropy bonus to promote exploration. Conversely, for simpler, low-uncertainty tasks, the policy model is encouraged for refinement and stabilization.

1) Quantifying Uncertainty via Policy Entropy: The intrinsic uncertainty of a policy model provides a potent proxy for task difficulty relative to the model's capability, which can be quantified on the fly by the entropy of its output distribution [8] [21] [33]. This means that high policy entropy suggests the model is struggling or exploring, indicative of a complex task that is beyond the model's current ability. In contrast, the low policy entropy represents that the model is confident, signifying a simpler task within the model's proficiency.

First, we compute the entropy of the model's prediction on the current sample. For each token position t in the token sequence $Y = \{y_1, y_2, \ldots, y_T\}$, the entropy of the predictive distribution over the vocabulary V is calculated by the following equation:

$$\begin{aligned} \mathcal{H}_t(y_t|X, q, y_{<t}) = -\sum_{v \in V} \pi_\theta(y_t = v|X, q, y_{<t}) \\ \cdot \log \pi_\theta(y_t = v|X, q, y_{<t}). \end{aligned} \quad (4)$$

We then average these per-token entropies across the entire sequence to obtain the final sentence entropy:

$$\mathcal{H}_{\text{seq}}(Y|X, q) = \frac{1}{T} \sum_{t=1}^{T} \mathcal{H}_t(y_t|X, q, y_{<t}), \quad (5)$$

where X is the input image set, and π_θ is the policy model.

Next, we measure the model's uncertainty for each sample by comparing its sequence entropy to a predefined threshold, which distinguishes between low and high uncertainty. A fixed threshold is suboptimal as it fails to adapt to the model's evolving reasoning capabilities during training. Thus, we use

an adaptive threshold, updated as a moving average of recent entropies, representing the model's average uncertainty based on recent samples. Specifically, we initialize the threshold by computing the median entropy of the training samples using the base model in inference mode. During model training, it is updated dynamically using the following Exponential Moving Average (EMA) formula:

$$\tau_s = \alpha \cdot \tau_{s-1} + (1-\alpha) \cdot \bar{\mathcal{H}}_s, \tag{6}$$

where τ_s and τ_{s-1} are adaptive thresholds at the current and previous steps, with τ_0 being the initial value. Hyperparameter α denotes the EMA decay factor, and $\bar{\mathcal{H}}_s$ indicates the average sequence entropy $\mathcal{H}_{\text{seq}}$ across the samples in the current batch.

2) Adaptive Advantage Shaping: The relationship between the sample-level entropy and adaptive threshold is then mapped to an uncertainty adjustment factor. Instead of a linear function, we utilize $tanh$ activation, which introduces beneficial non-linearity, and normalizes the deviation between the sample's entropy and the threshold into $[-1, 1]$. This normalization mitigates the influence of entropy deviations, preventing them from destabilizing the training process. The uncertainty adjustment factor for sample i is defined as:

$$\omega_{i,s} = \tanh\left(\gamma \cdot (\mathcal{H}_{seq,i,s} - \tau_s)\right), \tag{7}$$

where γ is the scaling hyperparameter that controls the steepness of the function.

The factor effectively transforms the uncertainty into a continuous, normalized signal bounded within $[-1, 1]$. We then leverage this factor to dynamically modulate the advantage. The final shaped advantage for sample i is as follows:

$$A_{i,s}^{\text{UADT}} = A_{i,s} + \lambda \cdot \omega_{i,s} \cdot \mathcal{H}_{seq,i,s}, \tag{8}$$

where $A_{i,s}$ stands for the original advantage, and λ is a scaling hyperparameter. This shaped advantage is then used to compute the policy optimization objective defined in Eq. 3, thereby achieving a dynamic, uncertainty-aware policy update.

3) Discussion and Analysis: UADT modulates the policy update by leveraging entropy to gauge sample-level uncertainty and advantage to assess action quality. We analyze its behavior across four scenarios, each defined by a combination of entropy and advantage:

- **High Uncertainty & Positive Advantage.** The model takes a beneficial action but is uncertain ($A_i > 0, \mathcal{H}_i > \tau_i$). UADT amplifies the shaped advantage A_i^{UADT}, acting as a bonus to encourage exploration.
- **High Uncertainty & Negative Advantage.** The model takes a negative action under high uncertainty ($A_i < 0, \mathcal{H}_i > \tau_i$) . The positive uncertainty factor promotes further exploration of challenging instances, preventing premature convergence, similar to hard sample mining.
- **Low Uncertainty & Positive Advantage.** The model is confident and correct ($\mathcal{H}_i < \tau_i, A_i > 0$). The shaped advantage A_i^{UADT} is slightly suppressed, preventing over-optimization on mastered samples and shifting focus to more uncertain tasks.
- **Low Uncertainty & Negative Advantage.** This scenario shows an overconfident mistake, where the model is highly confident but the action is wrong ($\mathcal{H}_i < \tau_i, A_i < 0$). UADT punishes these errors, encouraging mistake correction and enhancing model reliability.

UADT introduces an advanced and effective approach, offering several key strengths:

- **Adaptive Exploration.** It is critical for datasets with varying difficulty. UADT intelligently allocates its exploration budget to mitigate the dual risks of under-exploring on complex tasks and over-exploring on simple ones.
- **Automated and Self-Adaptive.** UADT leverages intrinsic model entropy as a signal without external supervision. The EMA-based mechanism ensures robustness against both evolving model proficiency and batch-level difficulty fluctuations.
- **Implementation Simplicity.** UADT requires minor code modifications to be incorporated into existing training pipelines, making it plug-and-play in diverse scenarios.

V. Experiments

A. Data and Experimental Setup

1) Training Data: OphthaReason is trained on the proposed MM-Retinal-Reason dataset, with strict separation between the training and evaluation sets at all stages to prevent data leakage. In the initial multimodal alignment stage, the model is trained on 72,861 samples from the image-caption subset of MM-Retinal-Reason (excluding 7,659 samples overlapping with the complex reasoning test set) and 9,437 samples from MM-Retinal [51] [50]. In the subsequent second and third training stages, the model is trained solely on the training splits, comprising 20,308 CoT and 28,238 VQA samples.

2) Evaluation Data: For a comprehensive evaluation, we assess the model on the MM-Retinal-Reason test set and two other external datasets. The external part includes the fundus and OCT branches of GMAI-MMBench [53], which are used for basic reasoning, and the selected ophthalmology-related samples of MedXpertQA-MM [58], which are used for complex reasoning. The composition of MM-Retinal-Reason test split is summarized in Tab. II. For each component dataset, we sample a maximum of 400 cases while preserving its original disease proportions. For those datasets dominated by healthy samples, we moderately perform downsampling to ensure a more substantial representation of diverse diseases.

3) Comparison Models: To validate OphthaReason's effectiveness and generalizability, we compare it against 14 MLLMs across basic and complex reasoning tasks, comprising proprietary and open-source general-purpose MLLMs, medical MLLMs, and RL-based medical reasoning MLLMs. Among them, we include FundusExpert and the fundus and OCT versions of Med-R1, which are specialized ophthalmic MLLMs.

4) Implementation Details: In the initial vision-language alignment stage, Qwen-based variant and Intern-based variant are trained for one epoch at learning rates of $2e-6$ and $2e-5$. For the second CoT supervision stage, variants are trained for two epochs with learning rates adjusted to $1e-6$ and $1e-5$. In the third RL stage, both variants are trained for two epochs using a learning rate of $1e-6$. We use AdamW as the optimizer throughout all training stages, and the sampling temperature

TABLE I: **Results on MM-Retinal-Reason basic reasoning subset of CFP and FFA modalities (%).** MM denotes MM-Retinal-Reason dataset. S-MCQ and M-MCQ denote Single-answer Multiple-Choice Questions and Multi-answer Multiple-Choice Questions. † The overlapping data between the MM-Retinal-Reason test split and the FundusExpert training set are removed. The best results are highlighted in **Bold**.

Model		Params	MM-CFP									MM-FFA		
			ID	OOD							AVG	ID	OOD	AVG
			S-MCQ	S-MCQ	M-MCQ									
			Acc	Acc	Jaccard	Acc	Precision	Recall	F1	AVG		Acc	Acc	
Open-Source General Models	GPT-4o [2]	-	59.50	62.06	45.81	30.79	53.61	54.41	51.69	47.26	56.27	24.00	57.50	40.75
	Gemini-2.5-Flash-Lite [9]	-	41.53	41.26	29.74	15.89	34.97	42.98	35.79	31.87	38.22	18.89	51.39	35.14
	LLaVA-Next [25]	8B	17.18	24.59	24.05	12.09	31.29	34.53	29.26	26.24	22.67	26.25	38.25	32.25
	Qwen2.5-VL-Instruct [3]	3B	31.07	32.62	26.21	13.59	34.87	32.90	31.21	27.75	30.48	29.75	29.00	29.38
	Qwen2.5-VL-Instruct [3]	7B	46.65	41.86	29.92	13.30	37.45	42.08	36.63	31.88	40.13	37.75	38.00	37.88
	InternVL-3 [7]	2B	54.42	52.35	27.52	15.27	32.19	37.18	32.37	28.90	45.22	26.00	44.50	35.25
Medical Models w/o RL	LLaVA-Med [24]	7B	31.29	33.22	25.88	19.07	34.88	25.88	28.48	26.84	30.45	26.53	28.95	27.74
	HealthGPT [28]	3.8B	42.36	38.08	32.24	18.42	38.22	47.16	38.40	34.89	38.44	26.75	32.00	29.38
	HuatuoGPT-Vision [5]	7B	57.38	50.22	38.07	28.25	50.46	38.32	41.75	39.37	49.06	39.25	45.75	42.50
	Lingshu [52]	7B	71.28	63.38	41.44	30.22	52.92	44.20	45.86	42.93	59.20	36.25	40.75	38.50
	FundusExpert† (CFP) [30]	8B	77.89	70.86	48.72	38.68	60.94	**52.52**	53.02	**50.78**	66.51	29.50	49.25	39.38
Medical Models w/ RL	MedVLM-R1 [37]	2B	31.73	30.57	27.70	5.44	32.92	48.12	36.54	30.14	30.81	27.00	26.00	26.50
	Med-R1 (CFP) [23]	2B	38.17	35.78	32.23	10.98	37.62	51.68	40.91	34.68	44.53	26.75	32.25	29.50
	QoQ-Med [10]	7B	59.63	51.95	34.33	16.74	39.81	48.93	41.40	36.24	49.27	40.50	32.00	36.25
	OphthaReason-Qwen	3B	74.25	71.08	42.11	31.01	51.42	46.30	46.46	43.46	62.93	64.75	45.00	54.88
	OphthaReason-Intern	2B	**83.75**	**73.78**	**49.48**	**38.70**	**61.33**	50.76	**53.52**	50.76	**69.43**	**74.25**	**61.75**	**68.00**

TABLE II: The composition of MM-Retinal-Reason test split.

Subset	Dataset Composition
CFP	**In-Domain:** PAPILA, PARAGUAY, ARIA, APTOS, HRF, DeepDRiD, G1020, AMD, PALM, ORIGA, Drishti-GS1, CHAKSU, Cataract, FUND-OCT, **Out-of-Domain:** MESSIDOR, IDRID, RFMid, STARE, ROC, Retina, SUSTech-SYSU, JICHI, EYEPACS, LAG, FIVES, E-ophta, REFUGE, DR1-2, ScarDat, ACRIMA, OIA-DDR
FFA	**In-Domain:** Angiographic **Out-of-Domain:** MPOS
OCT	**In-Domain:** GOALS, GAMMA1, STAGE1, STAGE2, OIMHS, OCTA_500, Large_Dataset_of_Labeled_OCT, DUKE_DME, glaucoma_detection, RetinalOCT_C8 **Out-of-Domain:** OCTDL, OCTID
Complex	PubMed Central (up to June 20, 2025)

is 1.0. The UADT hyperparameters γ and λ are empirically set to 0.5 and 1.0. We conduct training on 4 NVIDIA RTX A6000 GPUs and perform evaluation using vLLM framework [22] on 4 NVIDIA GeForce RTX 4090 GPUs.

B. Quantitative Results on Basic Reasoning Tasks

We evaluate the basic reasoning performance of OphthaReason under both In-Domain (ID) and Out-of-Domain (OOD) scenarios by conducting assessments across CFP, FFA, and OCT modalities. For the CFP modality, model performance is evaluated on both single-answer and multiple-answer multiple-choice questions. For the FFA and OCT modalities, only single-answer questions are included due to the scarcity of suitable public datasets.

1) In-Domain Effectiveness: As shown in Tab. I and Tab. III, OphthaReason significantly surpasses all competing models. Specifically, OphthaReason-Intern attains an accuracy of 83.75% for CFP modality, outperforming the second-best approach by a margin of 5.86%. This edge is also evident in FFA and OCT modalities, where our model exceeds the second-best models by 33.75% and 40.45%. This consistent state-of-the-art performance across modalities underscores the effectiveness of OphthaReason, establishing a solid foundation for its generalization and efficiency.

2) Out-of-Domain Generalization: Results in Tab. I and Tab. III also illustrate that OphthaReason consistently outperforms all competing models under the OOD settings. For CFP, it achieves 73.78% accuracy on single-answer MCQs and 50.76% on multi-answer MCQs. Notably, results on multi-answer MCQs are comparable to those of FundusExpert, despite OphthaReason using only one-quarter of the parameters (2B vs. 8B), and FundusExpert being more explicitly tailored for the CFP modality. Furthermore, OphthaReason maintains performance margins on both FFA and OCT modalities, demonstrating its overall superior generalization capability. We also conduct experiments on GMAI-MMBench. As illustrated in Fig. 4, OphthaReason remains superior in performance, competitive with FundusExpert and Lingshu, while outperforming most other models.

3) Higher Parameter Efficiency: OphthaReason-Intern-2B and OphthaReason-Qwen-3B are compared against similarly-sized models, much larger 7B-8B models, and massive-scale proprietary models like GPT-4o. The results in Tab. I and Tab. III reveal that OphthaReason achieves leading performance in a highly parameter-efficient manner. In the CFP modality, its average score of 69.43% not only surpasses specialized models like Lingshu-7B (59.20%) and FundusExpert-8B (66.51%), but also the proprietary GPT-4o (56.27%) and Gemini-2.5-Flash-Lite (38.22%). Similarly, in the FFA and OCT modalities, OphthaReason surpasses all baselines, achieving the best average scores of 68.00% and 65.06%.

TABLE III: **Results on MM-Retinal-Reason basic reasoning subset of OCT modality and complex reasoning subset(%).** MM denotes MM-Retinal-Reason dataset. The best results are highlighted in **Bold**.

Model		Params	MM-OCT			MM-Complex Reasoning						
			ID Acc	OOD Acc	AVG	Recall	BLEU	ROUGE-1	ROUGE-L	METEOR	BERTScore	AVG
Proprietary General Models	GPT-4o [2]	-	34.48	52.63	43.56	50.82	39.58	49.69	49.40	42.65	44.64	46.13
	Gemini-2.5-Flash-Lite [9]	-	30.78	49.06	39.92	39.28	35.95	40.98	40.88	32.76	39.47	38.22
Open-Source General Models	LLaVA-Next [25]	8B	29.22	30.75	29.99	12.10	10.18	14.04	14.04	9.39	10.67	11.74
	Qwen2.5-VL-Instruct [3]	3B	28.94	40.13	34.53	12.03	9.11	12.90	12.90	8.89	11.10	11.16
	Qwen2.5-VL-Instruct [3]	7B	28.73	38.50	33.62	17.93	13.94	18.97	18.90	13.07	16.51	16.55
	InternVL3 [7]	2B	30.61	32.13	31.37	16.70	13.26	17.91	17.83	12.46	15.00	15.53
Medical Models w/o RL	LLaVA-Med [24]	7B	28.09	27.85	27.97	18.88	4.74	9.27	8.92	12.13	7.22	10.19
	HealthGPT [28]	3.8B	30.75	32.63	31.69	20.77	17.61	22.97	22.87	16.15	20.60	20.16
	HuatuoGPT-Vision [5]	7B	41.42	53.63	47.53	21.84	13.80	20.78	20.56	16.63	15.59	18.20
	Lingshu [52]	7B	39.75	49.13	44.44	**26.67**	23.43	**28.30**	**28.12**	**21.31**	26.24	**25.68**
	FundusExpert (CFP) [30]	8B	31.45	45.75	38.60	13.09	10.96	15.12	15.05	9.85	12.16	12.70
Medical Models w/ RL	MedVLM-R1 [37]	2B	27.27	33.75	30.51	12.36	9.90	13.52	13.52	9.08	11.68	11.67
	Med-R1 (OCT/CFP) [23]	2B	28.87	26.88	27.88	10.04	8.01	11.17	11.17	7.30	9.91	9.60
	QoQ-Med [10]	7B	30.47	41.30	36.05	22.38	19.24	24.47	24.44	17.45	20.87	21.48
	OphthaReason-Qwen	3B	56.07	**54.63**	55.35	24.11	21.92	26.48	26.42	18.75	23.41	23.52
	OphthaReason-Intern	2B	**81.87**	48.25	**65.06**	25.65	**23.82**	27.55	27.52	20.79	**26.75**	25.35

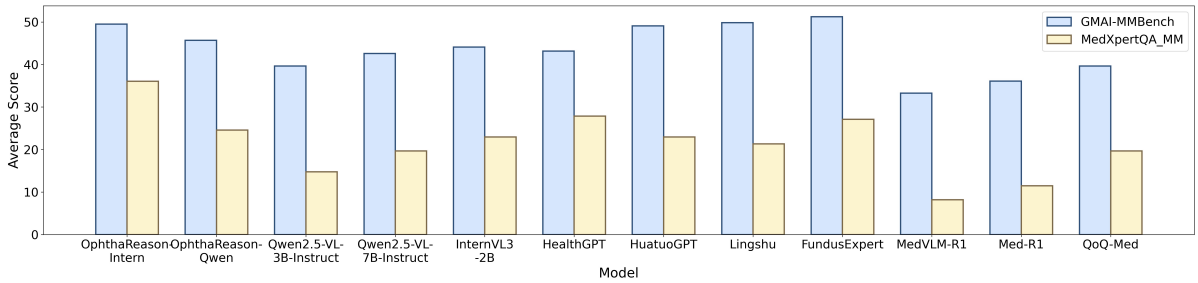

Fig. 4: Performance comparison on GMAI-MMBench (Fundus and OCT subsets) and MedXpertQA-MM (ophthalmology-related samples).

C. Quantitative Results on Complex Reasoning Tasks

In addition to the basic reasoning tasks, we further assess OphthaReason's advanced reasoning capabilities on the MM-Retinal-Reason Complex Reasoning subset, a challenging task designed to simulate real-world clinical scenarios, requiring models to integrate information from both multimodal images and detailed clinical information. Moreover, we also evaluate our model on the public MedXpertQA-MM dataset, another benchmark for complex reasoning. As it covers a broad range of medical domains, we only conduct the evaluation on ophthalmology-related samples.

1) Advanced Integrative Diagnostic Reasoning: As presented in Tab. III, OphthaReason achieves an average score of 25.35% across standard metrics evaluating answer accuracy and semantic alignment, outperforming a range of specialized medical models, such as HealthGPT (+5.19%) and QoQ-Med (+3.87%), as well as ophthalmic models, including FundusExpert (+12.65%) and Med-R1 fundus version (+15.75%), and is highly competitive with Lingshu. Comparison results on MedXpertQA-MM (Fig. 4) show that OphthaReason surpasses all the comparison models with an average score of 36.07%, exceeding HealthGPT by 8.20%, FundusExpert by 8.95%, and Lingshu by 14.75%.

2) Fundamental and Generalizable Representation: Although FundusExpert achieves competitive performance on CFP basic reasoning tasks (see Tab. I), it underperforms markedly on FFA, OCT basic reasoning tasks, and complex reasoning tasks (see Tab. I & III, and Fig. 4). This highlights that OphthaReason learned a more fundamental and robust representation of ophthalmic knowledge, demonstrating advanced ability to reason and diagnose from complex and multi-source clinical information. Moreover, OphthaReason's strong performance on the OOD dataset, MedXpertQA-MM, underscores its generalization ability on complex reasoning, supporting its potential for broader clinical applications.

3) Performance-Parameter Trade-off: OphthaReason consistently exhibits clear parameter efficiency in complex reasoning. Despite being 2–4 times smaller than competing models, it achieves results comparable to or superior to those larger counterparts. However, a notable performance gap exists when comparing our model to the proprietary model, such as GPT-4o. We attribute this disparity to the massive scale ($>$ 100B [1]) and diversity of the training data used by these models. This extensive and varied exposure is critical for complex reasoning. Nevertheless, deploying such large-scale models in real-world clinical use remains challenging, as most institutions are constrained by the extensive resources required. In contrast, our smaller-scale model offers a more feasible solution for practical adoption.

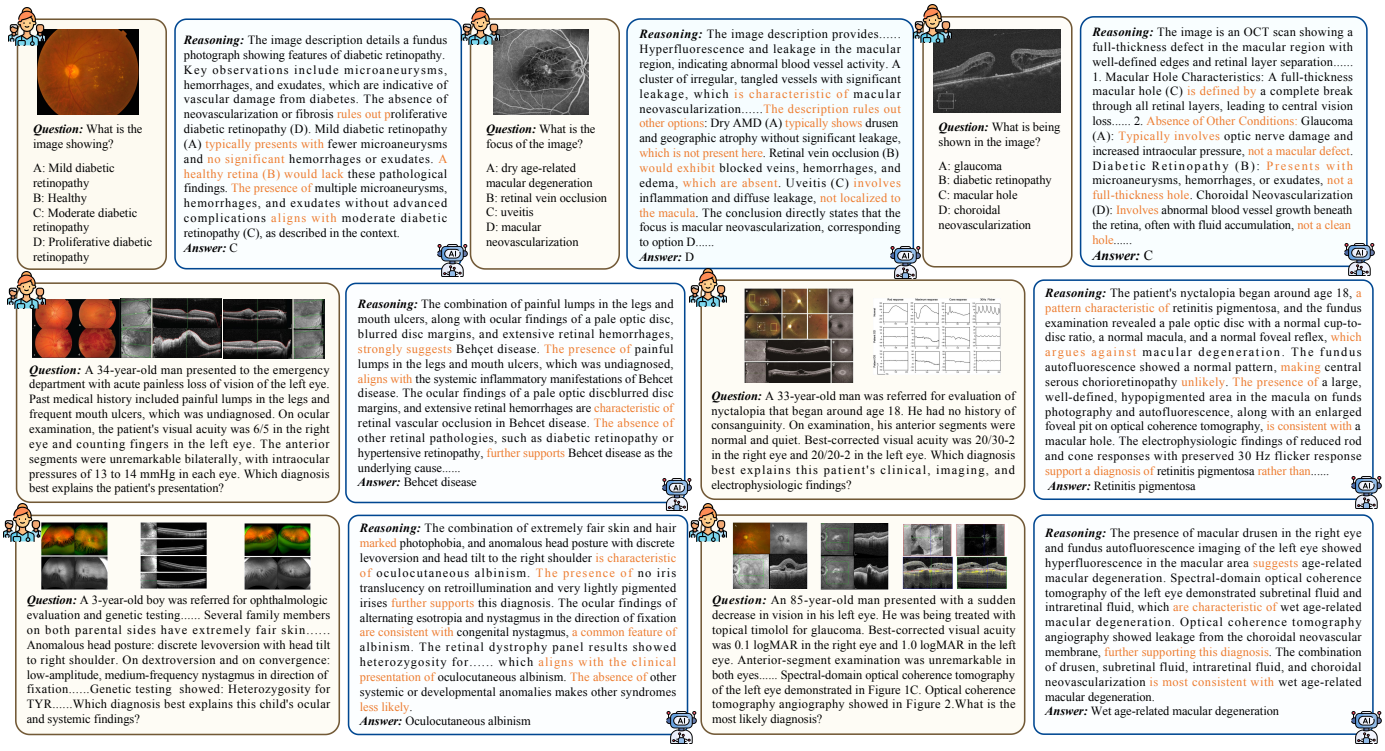

Fig. 5: Qualitative results of basic reasoning (first row) and complex reasoning (second and third rows). The content highlighted in orange indicates the key reasoning cues, reflecting the model's active process of evaluating evidence, eliminating differentials, and forming a diagnosis.

TABLE IV: **Ablation of different training stages and UADT on the MM-Retinal-Reason dataset**. The best results are highlighted in **Bold**.

Setting	CFP	FFA	OCT	Complex	AVG
Qwen2.5-VL-Instruct-3B	30.48	29.38	34.53	11.16	26.39
+ Supervised Fine-Tuning	37.31	20.00	32.34	3.25	23.23
+ Stage 3	55.81	43.75	43.34	17.10	40.00
+ Stage 2&3	59.79	52.38	48.25	**23.66**	46.02
+ Stage 1&2&3	62.07	**55.13**	50.86	22.52	47.65
+ Stage 1&2&3&UADT (ours)	**62.93**	54.88	**55.35**	23.52	**49.17**

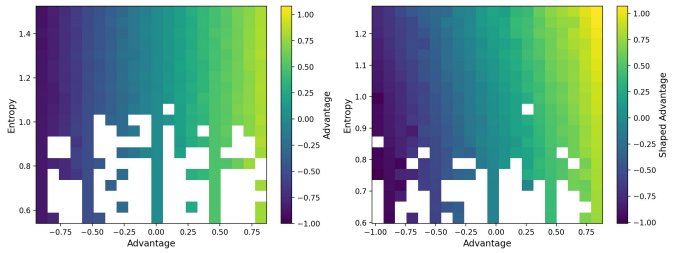

(a) Heatmap of Original Advantage (w/o UADT) (b) Heatmap of Shaped Advantage (w/ UADT)

Fig. 6: **Heatmaps of Advantage with and without UADT.** (a) Distribution of original advantage across entropy without UADT. (b) Distribution of shaped advantage after applying UADT. The color indicates the magnitude of the advantage, and white areas represent no data.

D. Qualitative Analysis of Case Studies

OphthaReason generates detailed, interpretable, and step-by-step reasoning traces for both basic and complex reasoning tasks. Qualitative examples are demonstrated in Fig. 5. OphthaReason excels at interpreting image content and identifying critical visual features (e.g., *"microaneurysms, hemorrhages, and exudates"* (top left) and *"irregular, tangled vessels with significant leakage"* (top center)). OphthaReason also exhibits proficiency in differential diagnosis by integrating multi-source clinically relevant information (e.g., *"aligns with the clinical presentation of oculocutaneous albinism"* (bottom left) and *"leakage from . . . , further supporting this diagnosis"* (bottom right)). These highlight OphthaReason's ability to integrate clinical evidence for reliable diagnostic reasoning.

E. Ablation Study

To validate the effectiveness of the three-stage training and the Uncertainty-Aware Dynamic Thinking (UADT), we conduct ablation studies by incrementally adding each component to the base model. The results are summarized in Tab. IV.

1) Impact of Different Training Stages: Qwen2.5-VL-Instruct base model obtains an average score of 26.39%, while Supervised Fine-Tuning (SFT) reduces the performance to 23.23%, indicating naive SFT leads the model to simply memorize patterns rather than reason from principles. In contrast, progressively applying the introduced specialized training stages boosts the model's performance. Reinforcement learning in Stage 3 brings the largest performance gain, increasing the average score by 13.61%, which is essential to enhance the model's reasoning ability. The contribution of CoT SFT in Stage 2 is also pivotal for developing the model's complex reasoning capabilities, which yields an improvement of 6.02%.

2) Impact of Uncertainty-Aware Dynamic Thinking (UADT): As shown in the last two rows of Tab. IV, the integration of UADT elevates the average score from 47.65%

to 49.17%. The improvements across all tasks underscore the criticality of UADT in enhancing model performance. To further investigate the underlying mechanism, we present a comparative visualization of the advantage heatmap in Fig. 6. As shown in the right panel, UADT dynamically modulates the advantage based on sample uncertainty. For high-entropy samples, UADT amplifies advantage to encourage exploration, evidenced by the color shift from blue/green to brighter green/yellow. Conversely, for low-entropy samples, UADT reduces the advantages, causing the corresponding regions to darken. Moreover, the comparison of the two panels reveals that UADT leads to a notable increase in sample density within the low-entropy region, particularly in the high-advantage area therein. This redistribution demonstrates that UADT effectively guides the policy model to not only generate correct answers but also with higher certainty, thereby improving the overall reliability and factuality.

VI. Conclusion

In this paper, we present MM-Retinal-Reason, the first multimodal ophthalmic dataset that spans the entire spectrum from visual perception to cognitive reasoning. Building on this foundation, we introduce OphthaReason, the first ophthalmology-specific multimodal reasoning model, trained through a three-stage pipeline comprising multimodal alignment, chain-of-thought supervised fine-tuning, and reinforcement learning. To accommodate varying levels of task complexity and simulate the progressive, adaptive reasoning essential in clinical diagnostics, we further propose an Uncertainty-Aware Dynamic Thinking (UADT) mechanism. Extensive experiments show that OphthaReason consistently outperforms 14 general-purpose and medical multimodal large language models across diverse modalities and reasoning scenarios. Future work may focus on scaling to larger foundation models and incorporating visual reasoning strategies, such as think-with-images, to enhance explainability in multimodal diagnosis.

Acknowledgments

This work was partially supported by the National Natural Science Foundation of China (Nos. 62476054, and 62172228), and the Fundamental Research Funds for the Central Universities (2242025K30024, and 2242025F10007).

References

[1] Abacha, A.B., Yim, W.w., Fu, Y., Sun, Z., Yetisgen, M., Xia, F., Lin, T.: Medec: A benchmark for medical error detection and correction in clinical notes. arXiv preprint arXiv:2412.19260 (2024)

[2] Achiam, J., Adler, S., Agarwal, S., Ahmad, L., Akkaya, I., Aleman, F.L., Almeida, D., Altenschmidt, J., Altman, S., Anadkat, S., et al.: Gpt-4 technical report. arXiv preprint arXiv:2303.08774 (2023)

[3] Bai, S., Chen, K., Liu, X., Wang, J., Ge, W., Song, S., Dang, K., Wang, P., Wang, S., Tang, J., et al.: Qwen2. 5-vl technical report. arXiv preprint arXiv:2502.13923 (2025)

[4] Ben Abacha, A., Hasan, S.A., Datla, V.V., Demner-Fushman, D., Müller, H.: Vqa-med: Overview of the medical visual question answering task at imageclef 2019. In: Proceedings of CLEF (Conference and Labs of the Evaluation Forum) 2019 Working Notes. 9-12 September 2019 (2019)

[5] Chen, J., Cai, Z., Ji, K., Wang, X., Liu, W., Wang, R., Hou, J., Wang, B.: Huatuogpt-o1, towards medical complex reasoning with llms. arXiv preprint arXiv:2412.18925 (2024)

[6] Chen, J., Gui, C., Ouyang, R., Gao, A., Chen, S., Chen, G.H., Wang, X., Zhang, R., Cai, Z., Ji, K., et al.: Huatuogpt-vision, towards injecting medical visual knowledge into multimodal llms at scale. arXiv preprint arXiv:2406.19280 (2024)

[7] Chen, Z., Wu, J., Wang, W., Su, W., Chen, G., Xing, S., Zhong, M., Zhang, Q., Zhu, X., Lu, L., et al.: Internvl: Scaling up vision foundation models and aligning for generic visual-linguistic tasks. In: Proceedings of the IEEE/CVF conference on computer vision and pattern recognition. pp. 24185–24198 (2024)

[8] Cheng, D., Huang, S., Zhu, X., Dai, B., Zhao, W.X., Zhang, Z., Wei, F.: Reasoning with exploration: An entropy perspective. arXiv preprint arXiv:2506.14758 (2025)

[9] Comanici, G., Bieber, E., Schaekermann, M., Pasupat, I., Sachdeva, N., Dhillon, I., Blistein, M., Ram, O., Zhang, D., Rosen, E., et al.: Gemini 2.5: Pushing the frontier with advanced reasoning, multimodality, long context, and next generation agentic capabilities. arXiv preprint arXiv:2507.06261 (2025)

[10] Dai, W., Chen, P., Ekbote, C., Liang, P.P.: Qoq-med: Building multimodal clinical foundation models with domain-aware grpo training. arXiv preprint arXiv:2506.00711 (2025)

[11] Deng, Y., Bansal, H., Yin, F., Peng, N., Wang, W., Chang, K.W.: Openvlthinker: An early exploration to complex vision-language reasoning via iterative self-improvement. arXiv preprint arXiv:2503.17352 (2025)

[12] Fan, Z., Liang, C., Wu, C., Zhang, Y., Wang, Y., Xie, W.: Chestx-reasoner: Advancing radiology foundation models with reasoning through step-by-step verification. arXiv preprint arXiv:2504.20930 (2025)

[13] Guo, D., Yang, D., Zhang, H., Song, J., Zhang, R., Xu, R., Zhu, Q., Ma, S., Wang, P., Bi, X., et al.: Deepseek-r1: Incentivizing reasoning capability in llms via reinforcement learning. arXiv preprint arXiv:2501.12948 (2025)

[14] Hoover, A.: Locating blood vessels in retinal images by piecewise threshold probing of a matched filter response. IEEE Transactions on Medical imaging **19**(3), 203–210 (2000)

[15] Hoover, A., Goldbaum, M.: Locating the optic nerve in a retinal image using the fuzzy convergence of the blood vessels. IEEE transactions on medical imaging **22**(8), 951–958 (2003)

[16] Hu, Y., Li, T., Lu, Q., Shao, W., He, J., Qiao, Y., Luo, P.: Omnimedvqa: A new large-scale comprehensive evaluation benchmark for medical lvlm. In: Proceedings of the IEEE/CVF Conference on Computer Vision and Pattern Recognition. pp. 22170–22183 (2024)

[17] Huang, W., Jia, B., Zhai, Z., Cao, S., Ye, Z., Zhao, F., Xu, Z., Hu, Y., Lin, S.: Vision-r1: Incentivizing reasoning capability in multimodal large language models. arXiv preprint arXiv:2503.06749 (2025)

[18] Huang, X., Shen, L., Liu, J., Shang, F., Li, H., Huang, H., Yang, Y.: Towards a multimodal large language model with pixel-level insight for biomedicine. In: Proceedings of the AAAI Conference on Artificial Intelligence. vol. 39, pp. 3779–3787 (2025)

[19] Jaech, A., Kalai, A., Lerer, A., Richardson, A., El-Kishky, A., Low, A., Helyar, A., Madry, A., Beutel, A., Carney, A., et al.: Openai o1 system card. arXiv preprint arXiv:2412.16720 (2024)

[20] Jing, P., Lee, K., Zhang, Z., Zhou, H., Yuan, Z., Gao, Z., Zhu, L., Papanastasiou, G., Fang, Y., Yang, G.: Reason like a radiologist: Chain-of-thought and reinforcement learning for verifiable report generation. arXiv preprint arXiv:2504.18453 (2025)

[21] Kadavath, S., Conerly, T., Askell, A., Henighan, T., Drain, D., Perez, E., Schiefer, N., Hatfield-Dodds, Z., DasSarma, N., Tran-Johnson, E., et al.: Language models (mostly) know what they know. arXiv preprint arXiv:2207.05221 (2022)

[22] Kwon, W., Li, Z., Zhuang, S., Sheng, Y., Zheng, L., Yu, C.H., Gonzalez, J., Zhang, H., Stoica, I.: Efficient memory management for large language model serving with pagedattention. In: Proceedings of the 29th symposium on operating systems principles. pp. 611–626 (2023)

[23] Lai, Y., Zhong, J., Li, M., Zhao, S., Yang, X.: Med-r1: Reinforcement learning for generalizable medical reasoning in vision-language models. arXiv preprint arXiv:2503.13939 (2025)

[24] Li, C., Wong, C., Zhang, S., Usuyama, N., Liu, H., Yang, J., Naumann, T., Poon, H., Gao, J.: Llava-med: Training a large language-and-vision assistant for biomedicine in one day. Advances in Neural Information Processing Systems **36**, 28541–28564 (2023)

[25] Li, F., Zhang, R., Zhang, H., Zhang, Y., Li, B., Li, W., Ma, Z., Li, C.: Llava-next-interleave: Tackling multi-image, video, and 3d in large multimodal models. arXiv preprint arXiv:2407.07895 (2024)

[26] Li, L., Xu, M., Wang, X., Jiang, L., Liu, H.: Attention based glaucoma detection: A large-scale database and cnn model. In: Proceedings of the IEEE/CVF conference on computer vision and pattern recognition. pp. 10571–10580 (2019)

[27] Li, S., Lin, T., Lin, L., Zhang, W., Liu, J., Yang, X., Li, J., He, Y., Song, X., Xiao, J., et al.: Eyecaregpt: Boosting comprehensive ophthalmology understanding with tailored dataset, benchmark and model. arXiv preprint arXiv:2504.13650 (2025)

[28] Lin, T., Zhang, W., Li, S., Yuan, Y., Yu, B., Li, H., He, W., Jiang, H., Li, M., Song, X., et al.: Healthgpt: A medical large vision-language model for unifying comprehension and generation via heterogeneous knowledge adaptation. arXiv preprint arXiv:2502.09838 (2025)

[29] Liu, S., Li, F., Zhang, H., Yang, X., Qi, X., Su, H., Zhu, J., Zhang, L.: Dab-detr: Dynamic anchor boxes are better queries for detr. arXiv preprint arXiv:2201.12329 (2022)

[30] Liu, X., Song, D.: Constructing ophthalmic mllm for positioning-diagnosis collaboration through clinical cognitive chain reasoning. arXiv preprint arXiv:2507.17539 (2025)

[31] Liu, Z., Sun, Z., Zang, Y., Dong, X., Cao, Y., Duan, H., Lin, D., Wang, J.: Visual-rft: Visual reinforcement fine-tuning. arXiv preprint arXiv:2503.01785 (2025)

[32] Luo, X., Zheng, R., Zheng, Q., Du, Z., Yang, S., Ding, M., Xu, Q., Liu, C., Shen, L.: A survey of multimodal ophthalmic diagnostics: From task-specific approaches to foundational models. arXiv preprint arXiv:2508.03734 (2025)

[33] MacKay, D.J.: Information-based objective functions for active data selection. Neural computation **4**(4), 590–604 (1992)

[34] Naren, O.S.: Retinal oct image classification - c8 (2021), Kaggle.https://doi.org/10.34740/KAGGLE/DSV/2736749

[35] OpenAI: Introducing o3 and o4-mini (Apr 2025), https://openai.com/index/introducing-o3-and-o4-mini/

[36] Pachade, S., Porwal, P., Thulkar, D., Kokare, M., Deshmukh, G., Sahasrabuddhe, V., Giancardo, L., Quellec, G., Mériaudeau, F.: Retinal fundus multi-disease image dataset (rfmid): A dataset for multi-disease detection research. Data **6**(2), 14 (2021)

[37] Pan, J., Liu, C., Wu, J., Liu, F., Zhu, J., Li, H.B., Chen, C., Ouyang, C., Rueckert, D.: Medvlm-r1: Incentivizing medical reasoning capability of vision-language models (vlms) via reinforcement learning. arXiv preprint arXiv:2502.19634 (2025)

[38] Pfob, A., Sidey-Gibbons, C., Barr, R.G., Duda, V., Alwafai, Z., Balleyguier, C., Clevert, D.A., Fastner, S., Gomez, C., Goncalo, M., et al.: The importance of multi-modal imaging and clinical information for humans and ai-based algorithms to classify breast masses (inspired 003): an international, multicenter analysis. European radiology **32**(6), 4101–4115 (2022)

[39] Rui, S., Chen, K., Ma, W., Wang, X.: Improving medical reasoning with curriculum-aware reinforcement learning. arXiv preprint arXiv:2505.19213 (2025)

[40] Shao, Z., Wang, P., Zhu, Q., Xu, R., Song, J., Bi, X., Zhang, H., Zhang, M., Li, Y., Wu, Y., et al.: Deepseekmath: Pushing the limits of mathematical reasoning in open language models. arXiv preprint arXiv:2402.03300 (2024)

[41] Shi, D., Zhang, W., Yang, J., Huang, S., Chen, X., Yusufu, M., Jin, K., Lin, S., Liu, S., Zhang, Q., et al.: Eyeclip: A visual-language foundation model for multi-modal ophthalmic image analysis. arXiv preprint arXiv:2409.06644 (2024)

[42] Silva-Rodriguez, J., Chakor, H., Kobbi, R., Dolz, J., Ayed, I.B.: A foundation language-image model of the retina (flair): Encoding expert knowledge in text supervision. Medical Image Analysis **99**, 103357 (2025)

[43] Su, Y., Li, T., Liu, J., Ma, C., Ning, J., Tang, C., Ju, S., Ye, J., Chen, P., Hu, M., et al.: Gmai-vl-r1: Harnessing reinforcement learning for multimodal medical reasoning. arXiv preprint arXiv:2504.01886 (2025)

[44] Tan, H., Ji, Y., Hao, X., Lin, M., Wang, P., Wang, Z., Zhang, S.: Reason-rft: Reinforcement fine-tuning for visual reasoning. arXiv preprint arXiv:2503.20752 (2025)

[45] Thapa, R., Wu, Q., Wu, K., Zhang, H., Zhang, A., Wu, E., Ye, H., Bedi, S., Aresh, N., Boen, J., et al.: Disentangling reasoning and knowledge in medical large language models. arXiv preprint arXiv:2505.11462 (2025)

[46] Wang, M., Lin, T., Lin, A., Yu, K., Peng, Y., Wang, L., Chen, C., Zou, K., Liang, H., Chen, M., et al.: Common and rare fundus diseases identification using vision-language foundation model with knowledge of over 400 diseases. CoRR (2024)

[47] Wang, Z., Guo, X., Stoica, S., Xu, H., Wang, H., Ha, H., Chen, X., Chen, Y., Yan, M., Huang, F., et al.: Perception-aware policy optimization for multimodal reasoning. arXiv preprint arXiv:2507.06448 (2025)

[48] Wu, J., Yang, H., Zeng, X., He, G., Chen, Z., Li, Z., Zhang, X., Ma, Y., Fang, R., Liu, Y.: Pathvlm-r1: A reinforcement learning-driven reasoning model for pathology visual-language tasks. arXiv preprint arXiv:2504.09258 (2025)

[49] Wu, K., Wu, E., Thapa, R., Wei, K., Zhang, A., Suresh, A., Tao, J.J., Sun, M.W., Lozano, A., Zou, J.: Medcasereasoning: Evaluating and learning diagnostic reasoning from clinical case reports. arXiv preprint arXiv:2505.11733 (2025)

[50] Wu, R., Su, N., Zhang, C., Ma, T., Zhou, T., Cui, Z., Tang, N., Mao, T., Zhou, Y., Fan, W., et al.: Mm-retinal v2: Transfer an elite knowledge spark into fundus vision-language pretraining. arXiv preprint arXiv:2501.15798 (2025)

[51] Wu, R., Zhang, C., Zhang, J., Zhou, Y., Zhou, T., Fu, H.: Mm-retinal: Knowledge-enhanced foundational pretraining with fundus image-text expertise. In: International Conference on Medical Image Computing and Computer-Assisted Intervention. pp. 722–732. Springer (2024)

[52] Xu, W., Chan, H.P., Li, L., Aljunied, M., Yuan, R., Wang, J., Xiao, C., Chen, G., Liu, C., Li, Z., et al.: Lingshu: A generalist foundation model for unified multimodal medical understanding and reasoning. arXiv preprint arXiv:2506.07044 (2025)

[53] Ye, J., Wang, G., Li, Y., Deng, Z., Li, W., Li, T., Duan, H., Huang, Z., Su, Y., Wang, B., et al.: Gmai-mmbench: A comprehensive multimodal evaluation benchmark towards general medical ai. Advances in Neural Information Processing Systems **37**, 94327–94427 (2024)

[54] Yu, S., Wang, H., Wu, J., Xie, C., Zhou, Y.: Medframeqa: A multi-image medical vqa benchmark for clinical reasoning. arXiv preprint arXiv:2505.16964 (2025)

[55] Zhang, W., Zhang, P., Guo, J., Cheng, T., Chen, J., Zhang, S., Zhang, Z., Yi, Y., Bu, H.: Patho-r1: A multimodal reinforcement learning-based pathology expert reasoner. arXiv preprint arXiv:2505.11404 (2025)

[56] Zhang, X., Wu, C., Zhao, Z., Lin, W., Zhang, Y., Wang, Y., Xie, W.: Pmc-vqa: Visual instruction tuning for medical visual question answering. arXiv preprint arXiv:2305.10415 (2023)

[57] Zhu, W., Li, X., Chen, X., Qiu, P., Vasa, V.K., Dong, X., Chen, Y., Lepore, N., Dumitrascu, O., Su, Y., et al.: Retinalgpt: A retinal clinical preference conversational assistant powered by large vision-language models. arXiv preprint arXiv:2503.03987 (2025)

[58] Zuo, Y., Qu, S., Li, Y., Chen, Z., Zhu, X., Hua, E., Zhang, K., Ding, N., Zhou, B.: Medxpertqa: Benchmarking expert-level medical reasoning and understanding. arXiv preprint arXiv:2501.18362 (2025)